International Journal of Heat and Mass Transfer 55 (2012) 5076–5086

Contents lists available at SciVerse ScienceDirect

International Journal of Heat and Mass Transfer

journal homepage: www.elsevier.com/locate/ijhmt

A heatline analysis of natural convection in a square inclined enclosure filled with a CuO nanofluid under non-uniform wall heating condition

Hakan F. Oztop [a], Moghtada Mobedi [b], Eiyad Abu-Nada [c,d], Ioan Pop [e,*]

[a] Department of Mechanical Engineering, Technology Faculty, Fırat University, Elazig, Turkey
[b] Department of Mechanical Engineering, Izmir Institute of Technology, Urla 35430, Izmir, Turkey
[c] Department of Mechanical Engineering, King Faisal University, Al-Ahsa 31982, Saudi Arabia
[d] Department of Mechanical Engineering, Hashemite University, Zarqa 13115, Jordan
[e] Faculty of Mathematics and Computer Science, Babes-Bolyai University, 400084 Cluj-Napoca, Romania

ARTICLE INFO

Article history:
Received 30 September 2011
Received in revised form 29 March 2012
Accepted 30 March 2012
Available online 7 June 2012

Keywords:
Heatline
Nanofluid
Natural convection
Enclosure

ABSTRACT

Heatline visualization technique is used to understand heat transport path in an inclined non-uniformly heated enclosure filled with water based CuO nanofluid. The cavity has square cross-section and it is non-uniformly heated from a wall and cooled from opposite wall while other walls are adiabatic. The governing equations which are continuity, momentum and energy equations are solved using finite volume method. The dimensionless heatfunction for nanofluid heat flow is defined and solved to determine heatline patterns. Calculations were performed for Rayleigh numbers of 10^3, 10^4 and 10^5, inclination angle of 0°, 30°, 60° and 90°, and nanoparticle fraction of 0, 0.02, 0.04, 0.06, 0.08 and 0.1. It is observed that heat transfer in the cavity increases by adding nanoparticles. The rate of increase is greater for the enclosures with low Rayleigh number. Visualization of heatline is successfully applied to nanoparticle convective flows. Based on the heatline patterns, three heat transfer regions are observed and discussed in details.

1. Introduction

Control of heat transfer in many energy systems is crucial due to the increase in energy prices. In recent years, nanofluids technology is proposed and studied by some researchers experimentally or numerically to control heat transfer in a process. The nanofluid can be applied to engineering problems, such as heat exchangers, cooling of electronic equipments and chemical processes. These applications and solution methods are reviewed by Kakac and Pramuanjaroenkij [1], Daungthongsuk and Wongwises [2], Trisaksri and Wongwises [3], Wang and Mujumdar [4], Putra et al. [5], Saidur et al. [6] and Lee et al. [7].

Natural convection heat transfer occurs in enclosures due to temperature difference and buoyancy forces. The problem was analyzed for enclosures filled with clear fluid [8] or nanofluid [9] and for the cases of constant temperature or constant heat flux. In recent years, effects of non-isothermal boundary conditions on natural convection in enclosure were analyzed by researchers due to its applications in solar systems or furnaces. In this context, Bilgen and Ben [10] performed study on the effects of non-isothermal boundary condition on natural convection for a rectangular cavity. In their study, two cases were considered: in the first case, the lower part was heated while the upper part was cooled. In the second case, the upper part of cavity was heated while the lower part was cooled. Natarajan et al. [11] conducted a study using a penalty finite element analysis with bi-quadratic elements to investigate the effects of uniform and non-uniform heating of bottom wall on natural convection flows in a trapezoidal cavity. Moreover, two-dimensional laminar natural convection in enclosures with three flat and one wavy wall, one of which was exposed to sinusoidal temperature profile, was studied by Dalal and Das [12]. Basak et al. [13] solved the governing equations using the finite element method to study the effects of thermal boundary condition in square enclosures. They numerically tested the effects of Prandtl number and observed that the non-uniform heating of the bottom wall produced greater heat transfer rates at the center of the bottom wall than the uniform heating case for the whole range of Rayleigh numbers. However, average Nusselt numbers showed lower heat transfer rates for the non-uniform heating. Varol et al. [14] investigated the effects of sinusoidally varying temperature on natural convection in a rectangular enclosures filled with porous media, numerically. Sarris et al. [15] numerically studied the natural convection in a square cavity with non-isothermal temperature gradient on top wall. The problem of non-isothermal boundary conditions was extended to nanofluid by Oztop et al. [16]. In their case, comparison of Al_2O_3 and TiO_2 nanoparticle was performed from heat transfer enhancement point of view.

* Corresponding author.
E-mail address: popm.ioan@yahoo.co.uk (I. Pop).

0017-9310/$ - see front matter © 2012 Elsevier Ltd. All rights reserved.
http://dx.doi.org/10.1016/j.ijheatmasstransfer.2012.05.007

Nomenclature

c_p	specific heat at constant pressure (J kg^{-1} K^{-1})
g	gravitational acceleration (m s^{-2})
H	height of the enclosure (m)
h	local heat transfer coefficient (W m^{-2} K^{-1})
$\mathbf{J}$	heat transfer vector (W m^{-2} K^{-1})
k	thermal conductivity (W m^{-1} K^{-1})
Nu	Nusselt number
Pr	Prandtl number
q_w	heat flux (W m^{-2})
Ra	Rayleigh number
T	temperature of the nanofluid (K)
u', v'	dimensional velocity components along x' and y' directions (m s^{-1})
U, V	dimensionless velocity components along x and y directions
W	width of the enclosure (m)
x', y'	dimensional coordinates (m)
x, y	dimensionless coordinates

Greek symbols

α	fluid thermal diffusivity (m^2 s^{-1})
β	thermal expansion coefficient (K^{-1})
ε	numerical tolerance
φ	nanoparticle volume fraction
ϕ	inclination angle
μ	dynamic viscosity (N s m^{-2})
ν	kinematic viscosity (m^2 s^{-1})
ω	dimensional vorticity (s^{-1})
Ω	dimensionless vorticity
π	dimensional heatfunction (W/m)
Π	dimensionless heatfunction
θ	dimensionless temperature
ρ	density (kg m^{-3})
ψ	dimensional streamfunction (m^2 s^{-1})
Ψ	Dimensionless streamfunction

Subscripts

avg	average
c	cold
f	fluid
h	hot
nf	nanofluid
s	solid
w	wall

The heatline visualization technique is a useful tool to observe heat transfer path in a heat transfer domain. The technique was first proposed by Kimura and Bejan [17] to visualize heat transport for convective heat transfer. A detailed review on the application of heatline visualization method was presented by Costa [18]. Hakyemez et al. [19] used heatline visualization technique to show the path of heat transfer in a cavity. In their geometry, a thermal barrier was used in the ceiling wall. Varol et al. [20] made a numerical work to visualize heat transfer in a non-isothermally heated triangular cavity filled with porous media. They observed that the non-isothermal wall changes the heat transport way. Basak et al. [21] studied the natural convection in porous trapezoidal enclosures for uniformly or non-uniformly heated bottom wall by presenting, streamlines, isotherms and heatlines. They observed that heatlines are affected with Darcy number.

The main objective of the present study is to analyze heat and fluid flow in an inclined non-uniformly heated enclosure filled with CuO nanofluids. The effects of nanoparticle fraction and inclination angle on heat transfer through the enclosure are investigated. Isotherms, streamlines and heatlines are plotted for enclosures with different Rayleigh numbers, nanoparticle fractions and inclination angles to discuss the changes of average Nusselt number. Moreover, the distributions of local Nusselt number along the hot and cold walls are presented to support the discussions. The variations of average Nusselt number with Rayleigh number, nanoparticle fraction and inclination angle are presented via tables. Based on performed literature survey, this is the first study on application of heatfunction on heat transfer in a nanoparticle fluid flow. Heatfunction for a flow field containing mixture of nanoparticles and pure fluid is defined and applied successfully.

2. Problem definition

The considered enclosure is illustrated in Fig. 1. It is a square enclosure whose height and width are identical while inclination angle ϕ varies from 0° to 90°. The left side of enclosure is heated linearly and the right vertical wall is kept at constant temperature when $\phi = 0°$. The minimum temperature of the heated wall is at the top of wall and it is identical with cold wall temperature shown by T_c. The maximum temperature of the hot wall is at the bottom of wall represented by T_h. The horizontal walls are adiabatic and gravity acts in vertical direction. The cavity is filled with water based CuO nanofluid.

3. Governing equations

Two dimensional, laminar, steady flow of incompressible fluid is assumed in this work. The governing equations are written in vorticity-streamfunction mode as

Vorticity

$$\frac{\partial}{\partial x'}\left(\omega\frac{\partial\psi}{\partial y'}\right)-\frac{\partial}{\partial y'}\left(\omega\frac{\partial\psi}{\partial x'}\right)=\frac{\mu_{nf}}{\rho_{nf}}\left(\frac{\partial^2\omega}{\partial x'^2}+\frac{\partial^2\omega}{\partial y'^2}\right)+\frac{(\varphi\rho_s\beta_s+(1-\varphi)\rho_f\beta_f)}{\rho_{nf}}g\left(\frac{\partial T}{\partial x'}\cos\phi-\frac{\partial T}{\partial y'}\sin\phi\right) \quad (1)$$

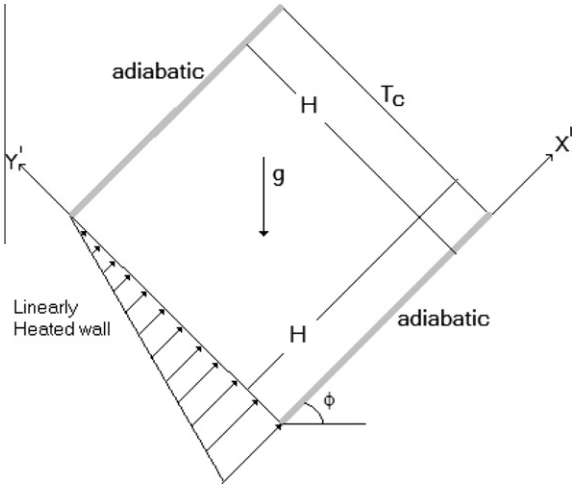

Fig. 1. Physical model and coordinate system.

Energy

$$\frac{\partial}{\partial x'}\left(T\frac{\partial \psi}{\partial y'}\right)-\frac{\partial}{\partial y'}\left(T\frac{\partial \psi}{\partial x'}\right)=\frac{\partial}{\partial x'}\left[\alpha_{nf}\frac{\partial T}{\partial x'}\right]+\frac{\partial}{\partial y'}\left[\alpha_{nf}\frac{\partial T}{\partial y'}\right] \tag{2}$$

streamfunction

$$\frac{\partial^2 \psi}{\partial x'^2}+\frac{\partial^2 \psi}{\partial y'^2}=-\omega \tag{3}$$

where x' and y' are the Cartesian coordinates along the inclined wall and normal to it, respectively, T is the temperature of the nanofluid, ω is the vorticity, ψ is the streamfunction, which is defined as $u'=\partial\psi/\partial y'$ and $v'=-\partial\psi/\partial x'$, and the physical meaning of other quantities is given in Nomenclature. Further, α_{nf} is the effective thermal diffusivity of the nanofluids, μ_{nf} is the effective dynamic viscosity of the nanofluids and ρ_{nf} is the effective density of the nanofluids, which are defined as

$$\alpha_{nf}=\frac{k_{nf}}{(\rho c_p)_{nf}},\quad \mu_{nf}=\frac{\mu_f}{(1-\varphi)^{2.5}},\quad \rho_{nf}=(1-\varphi)\rho_f+\varphi\rho_s \tag{4}$$

Here $(\rho c_p)_{nf}$ is the heat capacitance of the nanofluid expressed by Abu-Nada [22] and Khanafer et al. [23] as

$$(\rho c_p)_{nf}=(1-\varphi)(\rho c_p)_f+\varphi(\rho c_p)_s \tag{5}$$

and k_{nf} is the effective thermal conductivity of the nanofluid which can be approximated for spherical nanoparticles by the Maxwell–Garnetts model as

$$\frac{k_{nf}}{k_f}=\frac{k_s+2k_f-2\varphi(k_f-k_s)}{k_s+2k_f+\varphi(k_f-k_s)} \tag{6}$$

For a nanofluid with a specified nanoparticle volume fraction φ, the values of $(\rho c_p)_{nf}$ and k_{nf} are assumed to be constant. This model is found to be appropriate for studying heat transfer enhancement using nanofluids [24,22,25]. The viscosity of the nanofluid μ_{nf} can be approximated as viscosity of a base fluid μ_f containing dilute suspension of fine spherical particles and it is has been given by Brinkman [26].

The following dimensionless variables are introduced to obtain the dimensionless form of the governing equations:

$$x=\frac{x'}{H},\quad y=\frac{y'}{H},\quad \Omega=\frac{\omega H^2}{\alpha_f},\quad \Psi=\frac{\psi}{\alpha_f},\quad U=\frac{u'H}{\alpha_f},\quad V=\frac{v'H}{\alpha_f},\quad \theta=\frac{T-T_c}{T_h-T_c} \tag{7}$$

Thus, Eqs. (1)–(3) can be written in dimensionless form as

$$\frac{\partial}{\partial x}\left(\Omega\frac{\partial \Psi}{\partial y}\right)-\frac{\partial}{\partial y}\left(\Omega\frac{\partial \Psi}{\partial x}\right)=\left[\frac{\Pr}{(1-\varphi)^{0.25}((1-\varphi)+\varphi\frac{\rho_s}{\rho_f})}\right]\left(\frac{\partial^2\Omega}{\partial x^2}+\frac{\partial^2\Omega}{\partial y^2}\right)+Ra\Pr\left[\frac{1}{\frac{(1-\varphi)}{\varphi}\frac{\rho_f}{\rho_s}+1}\frac{\beta_s}{\beta_f}+\frac{1}{\frac{\varphi}{(1-\varphi)}\frac{\rho_f}{\rho_s}+1}\right]\left(\frac{\partial\theta}{\partial x}\cos\phi-\frac{\partial\theta}{\partial y}\sin\phi\right) \tag{8}$$

$$\frac{\partial}{\partial x}\left(\theta\frac{\partial \Psi}{\partial y}\right)-\frac{\partial}{\partial y}\left(\theta\frac{\partial \Psi}{\partial x}\right)=\frac{\partial}{\partial x}\left(\lambda\frac{\partial\theta}{\partial x}\right)+\frac{\partial}{\partial y}\left(\lambda\frac{\partial\theta}{\partial y}\right) \tag{9}$$

$$\frac{\partial^2\Psi}{\partial x^2}+\frac{\partial^2\Psi}{\partial y^2}=-\Omega \tag{10}$$

where the dimensionless streamfunction Ψ is defined as $U=\partial\Psi/\partial Y$ and $V=-\partial\Psi/\partial X$, Pr is the Prandtl number, Ra is the Rayleigh number and λ is a constant, which are defined as

$$\Pr=\frac{\nu_f}{\alpha_f},\quad Ra=\frac{g\beta_f H^3(T_h-T_c)}{\nu_f\alpha_f},\quad \lambda=\frac{\frac{k_{nf}}{k_f}}{(1-\varphi)+\varphi\frac{(\rho c_p)_s}{(\rho c_p)_f}} \tag{11}$$

The dimensionless boundary conditions based on $\phi=0^\circ$ are written as:

$$\begin{aligned}
&-\text{ on the left wall } x=0: \quad \Psi=0,\quad \Omega=-\frac{\partial^2\Psi}{\partial x^2},\quad \theta=1-y\\
&-\text{ on the right wall } x=1: \quad \Psi=0,\quad \Omega=-\frac{\partial^2\Psi}{\partial x^2},\quad \theta=0\\
&-\text{ on the top and bottom walls}: \quad \Psi=0,\quad \Omega=-\frac{\partial^2\Psi}{\partial y^2},\quad \frac{\partial\theta}{\partial y}=0
\end{aligned} \tag{12}$$

4. Heat function

For a two dimensional steady and incompressible nanofluid flow without heat generation, the components J_x and J_y of the heat flux vector **J**, containing the diffusion and convection transport, in the x and y directions can be written as

$$J_x=(\rho c_p)_{nf}u'(T-T_c)-k_{nf}\frac{\partial T}{\partial x'},\quad J_y=(\rho c_p)_{nf}v'(T-T_c)-k_{nf}\frac{\partial T}{\partial y'} \tag{13}$$

The value of the total heat flux vector **J** is the vectorial sum of the two heat flux components;

$$\vec{J}=J_x\vec{i}+J_y\vec{j} \tag{14}$$

where the vectors **i** and **j** represent Cartesian unit vectors. The application of energy conservation law on a finite volume in the nanofluid flow field by using Eq. (13) yields the energy equation for the nano fluid flow:

$$\frac{\partial J_x}{\partial x'}+\frac{\partial J_y}{\partial y'}=(\rho c_p)_{nf}\left(\frac{\partial uT}{\partial x'}+\frac{\partial vT}{\partial y'}\right)-k_{nf}\left(\frac{\partial^2 T}{\partial x'^2}+\frac{\partial^2 T}{\partial y'^2}\right)=0 \tag{15}$$

By defining π as a continuous scalar function, whose the first and second derivatives are also continuous, the dimensional heatfunction can be written in a differential form [17];

$$-\frac{\partial\pi}{\partial x'}=J_y,\quad \frac{\partial\pi}{\partial y'}=J_x \tag{16}$$

By substituting of Eq. (16) into Eq. (13), taking derivatives with respect to y' and x', and subtracting the resulting equations from each other, the following elliptic partial differential equation for the heatfunction is obtained

$$\frac{\partial^2\pi}{\partial x'^2}+\frac{\partial^2\pi}{\partial y'^2}=(\rho c_p)_{nf}\left[\frac{\partial}{\partial y'}(u'T)-\frac{\partial}{\partial x'}(v'T)\right] \tag{17}$$

The convection term which appears on the right side of Eq. (17) acts as a source term. It should be mentioned that the defined heatfuncton π includes both the diffusion and convection modes of heat transfer. The solution of Eq. (17) yields the values of the dimensional heatfunction for the all nodes of a computational domain and contour plots of the heatfunction values provides dimensional heatline patterns. By employing the dimensionless parameters presented by Eq. (7), the dimensionless heatfunction can be written as:

$$-\frac{\partial\Pi}{\partial x}=\frac{(\rho c_p)_{nf}}{(\rho c_p)_f}(V\theta)-\frac{k_{nf}}{k_f}\frac{\partial\theta}{\partial y},\quad \frac{\partial\Pi}{\partial y}=\frac{(\rho c_p)_{nf}}{(\rho c_p)_f}(U\theta)-\frac{k_{nf}}{k_f}\frac{\partial\theta}{\partial x} \tag{18}$$

where Π is the dimensionless heatfunction as

$$\Pi=\frac{\pi}{(T_h-T_c)k_f} \tag{19}$$

By performing the mathematical manipulations similar to the procedure for obtaining Eq. (17) from Eq. (16), the following dimensionless heatfunction equation can be obtained from Eq. (18)

$$\frac{\partial^2 \Pi}{\partial x^2}+\frac{\partial^2 \Pi}{\partial y^2}=\frac{(\rho c_p)_{nf}}{(\rho c_p)_f}\left[\frac{\partial}{\partial y}(U\theta)-\frac{\partial}{\partial x}(V\theta)\right] \tag{20}$$

The boundary conditions for dimensionless heatfunction equation (20) are obtained from the integration of Eq. (18) along the considered boundary. For instance, the following equation can be used to determine the values of heatfunction at the left wall of the cavity with $\phi = 0^\circ$ [19]

$$x=0,\ 0<y\leqslant 1: \quad \Pi(0,y)=\Pi(0,0)-\frac{k_{nf}}{k_f}\int_0^y\left(\frac{\partial\theta}{\partial x}\right)_{x=0}dy \tag{21}$$

The derivative of the dimensionless temperature at a wall with respect to its normal direction is defined as local Nusselt number, hence, Eq. (21) can also be written in the following form

$$x=0,\ 0<y\leqslant 1: \quad \Pi(0,y)=\Pi(0,0)-\int_0^y Nu(0,y)dy \tag{22}$$

5. Analysis of heat transfer

After solving vorticity, energy and streamfunction equations, and obtaining Ψ, Ω and θ distributions in the enclosure, indicators for dimensionless heat transfer rate should be obtained. The local Nusselt number can be expressed as:

$$Nu_y=\frac{h_y H}{k_f} \tag{23}$$

The local heat transfer coefficient h_y is expressed as

$$h_y=\frac{q_w}{T_h-T_c} \tag{24}$$

where T_h is maximum temperature of the hot wall and T_c is the cold wall temperature. On the other hand, the thermal conductivity for a nanofluid is defined as

$$k_{nf}=-\frac{q_w}{\partial T/\partial x} \tag{25}$$

By substituting Eqs. (25) and (24) into Eq. (23), and using the dimensionless quantities (7), the local Nusselt numbers on the hot and cold walls (Nu_c and Nu_h) for a cavity with $\phi = 0^\circ$ are written as

$$Nu_h=-\left(\frac{k_{nf}}{k_f}\right)\left(\frac{\partial\theta}{\partial x}\right)_{x=0}, \quad Nu_c=-\left(\frac{k_{nf}}{k_f}\right)\left(\frac{\partial\theta}{\partial x}\right)_{x=1} \tag{26}$$

The average Nusselt number Nu_{avg} is defined as:

$$Nu_{avg}=\int_0^1\sqrt{[Nu_y]^2}dy \tag{27}$$

For convenience, a normalized average Nusselt number $\bar{N}u_{avg}$ is defined as the ratio of average Nusselt number in enclosure having nanoparticles to that of pure water that is

$$Nu^*_{avg}(\phi,\varphi)=\frac{Nu_{avg}(\phi,\varphi)}{Nu_{avg}(\phi,\varphi=0)} \tag{28}$$

The use of normalized average Nusselt number $\bar{N}u_{avg}(\phi,\varphi)$ gives more insight on the heat transfer enhancement on the heated or cooled wall. The normalized average Nusselt number is used as an indicator of heat transfer enhancement since an increase in Nusselt number corresponds to an enhancement in heat transfer.

6. Numerical details

Eqs. (8)–(10) with corresponding boundary conditions given in Eq. (12) are solved using the finite volume approach [27,28]. The diffusion term in the vorticity and energy equations is approximated by a second-order central difference scheme which gives a stable solution. Furthermore, a second order upwind differencing scheme is adopted for the convective terms. The resulted algebraic equations are solved using successive over/under relaxation method. Successive under relaxation is used due to the non-linear nature of the governing equations especially for the vorticity equation at high Rayleigh numbers. The convergence criterion is defined by the following expression [29]:

$$\varepsilon=\frac{\sum_{j=1}^{j=M}\sum_{i=1}^{i=N}|\phi^{n+1}-\phi^n|}{\sum_{j=1}^{j=M}\sum_{i=1}^{i=N}|\phi^{n+1}|}<10^{-6} \tag{29}$$

where ε is the tolerance; M and N are the number of grid points in the x and y directions, respectively [30]. An accurate representation of vorticity at the surface is the most critical step in the streamfunction-vorticity formulation. A second order accurate formula is used for the vorticity boundary condition. For example, the vorticity at the bottom wall is expressed as [9]:

$$\Omega=-\frac{(8\Psi_{i,2}-\Psi_{i,1})}{2(\Delta y)^2} \tag{30}$$

where $\Psi_{i,2}$ and $\Psi_{i,1}$ are two neighboring nodes in y direction. 1/3rd Simpson's rule of integration is implemented to take integral of local Nusselt and obtain the average Nusselt number.

7. Results and discussion

Visualization of heat transport using heatline technique is presented in this study for non-isothermally heated square inclined enclosure filled with water/CuO nanofluid. The governing parameters are Rayleigh number, nanofluid fraction ratio and inclination angle of enclosure. Results are presented by streamlines, isotherms, heatlines, local and average Nusselt numbers, normalized Nusselt number and velocity profiles.

Fig. 2 compares the streamline (on the left), isotherm (on the middle) and heatline (on the right) for the enclosures with $Ra = 10^3$ and 10^5 for $\varphi = 0$ (classical fluids) and 0.1. As seen for two Rayleigh numbers, there are differences between the isotherms, streamline and heatline patterns in the enclosures for $\varphi = 0$ and 0.1 due to adding of nanoparticles.

Fig. 3 shows the streamline, isotherm and heatline for the enclosure with $Ra = 10^5$ and $\phi = 0^\circ$ for two values of φ as 0.02 and 0.08. Two cells are observed in the cavity. The first one (main cell) is the clockwise flow circulation which is dominant in the most part of the cavity while a weak counter clockwise flow is observed at the left top corner of cavity. The linear change of temperature at the left wall of the cavity causes the formation of the weak closed cells. The strength of the flow increases with nanoparticle volume fraction. The minimum value of Ψ is -13.54 for the cavity with $\varphi = 0.02$ and it rises to -15.203 for the cavity with $\varphi = 0.08$. The isotherm patterns for two nanoparticle volume fractions are similar to each others. The isotherm lines at the right region of the enclosure are parallel to the cold wall while isotherms cross the left wall. The heat transfer between cold and hot regions of the enclosure cannot be well understood by using isotherm patterns. That is why the heatline patterns of the enclosure are plotted and presented at the third column of the Fig. 3. As is seen from the heatline patterns, for the enclosure with nanoparticle fractions, heat transfer region in the enclosure can be divided into three regions. The first heat transfer region is on the left side of the cavity and it is shown by dark gray. As seen from heatline pattern in this region, heat is transferred from middle part of the hot wall to the top region of the same wall due to non-uniform wall temperature. The second heat transfer region is shown by light gray color. In this region, heat is transferred from hot to the cold wall. As seen from the heatline patterns, heat received by the cold wall is transferred

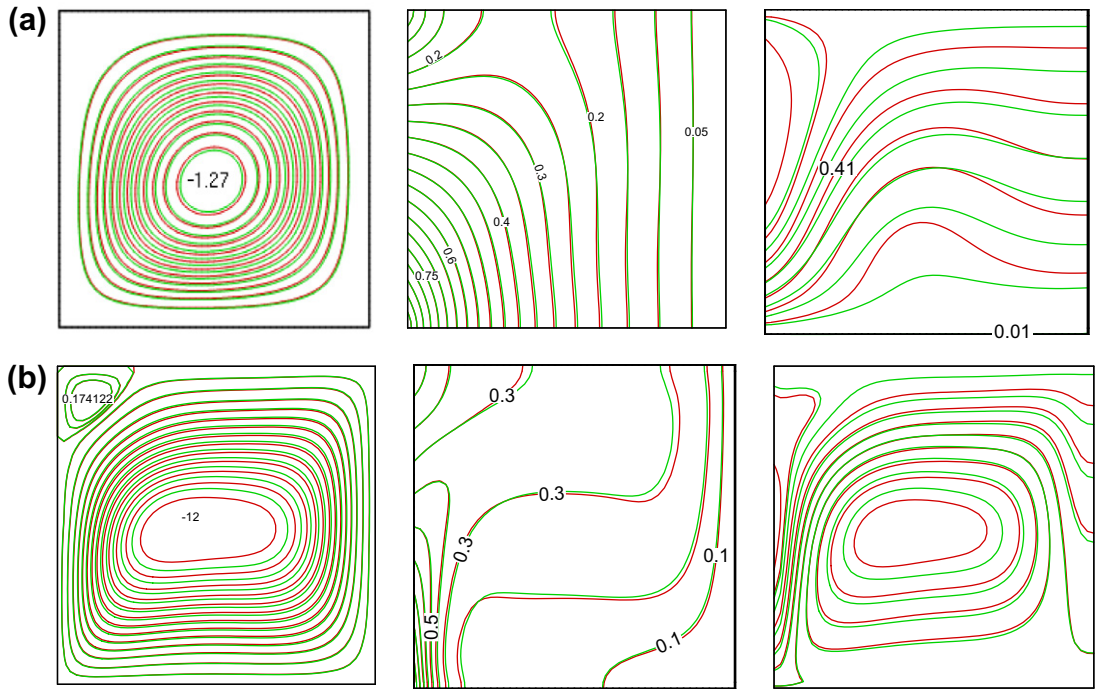

Fig. 2. Streamlines (on the left), isotherms (on the middle) and heatlines (on the right) for $\varphi = 0$ and $\varphi = 0.1$, (a) Ra = 10^3 and (b) Ra = 10^5 (red line: water, green line: water/CuO nanofluid). (For interpretation of the references to color in this figure legend, the reader is referred to the web version of this article.)

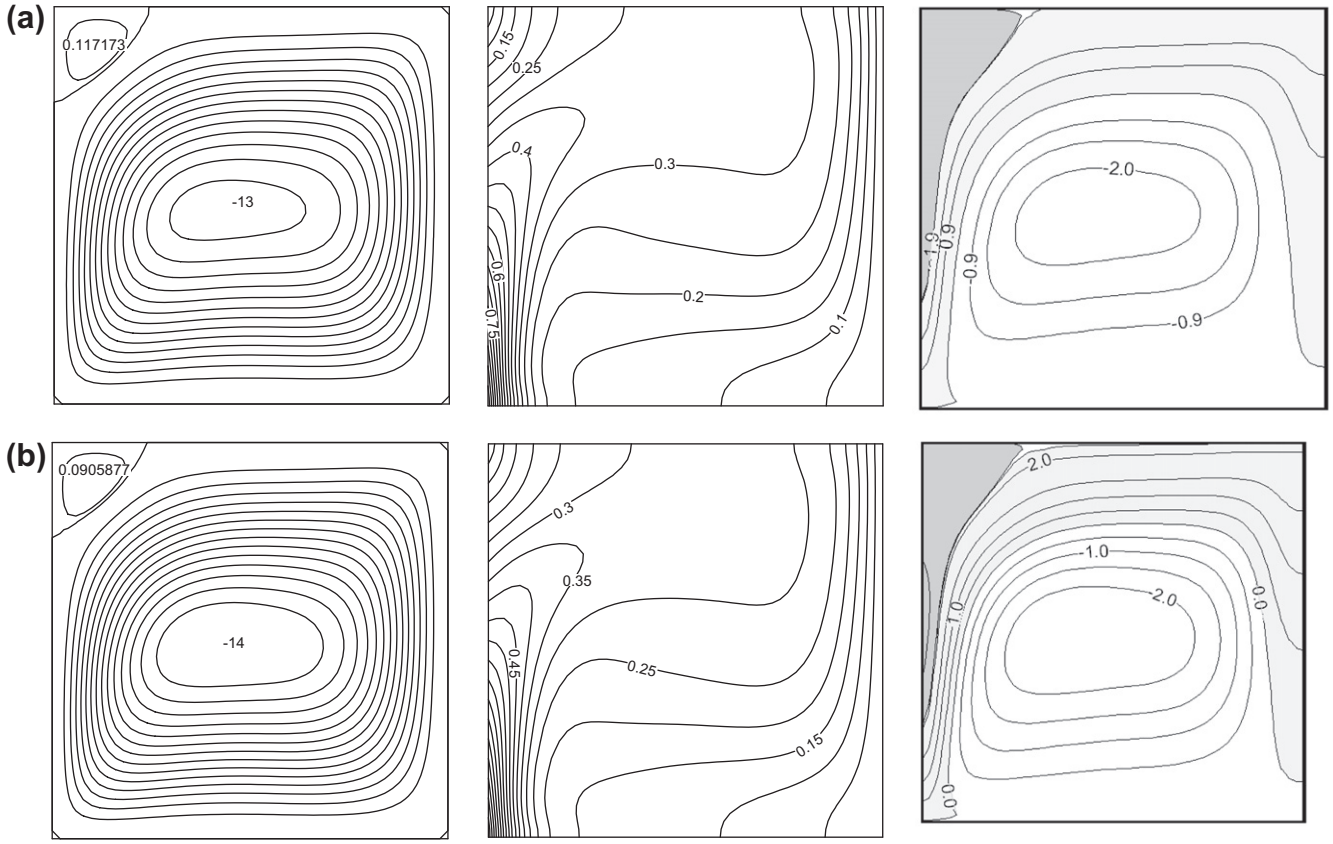

Fig. 3. Streamlines (on the left), isotherms (on the middle) and heatlines (on the right) for Ra = 10^5 and $\phi = 0°$, (a) $\varphi = 0.02$ and (b) $\varphi = 0.08$.

from the bottom of the hot wall. The third heat transfer region is not colored and it is white. In this region, heat is rotated in closed cells without having any function on heat transfer between walls. This region is called as passive region. The values of heatline contours are negative in the third region showing reverse heat flux rotation. Although a significant difference between the heatline

contours of enclosures having different nanoparticle fraction is not observed, considerable differences between the minimum and maximum values of heatfunction exist. For the cavity with $\varphi = 0.02$, the values of Π_{min} and Π_{max} are -2.35 and 2.45, respectively. The values of Π_{min} and Π_{max} become as -2.60 and 2.75 for the cavity with $\varphi = 0.08$. The increase of $\Pi_{max} - \Pi_{min}$ by increase of φ shows that heat transfer in the cavity is enhanced by adding of nanoparticle fraction.

Fig. 4 shows the streamlines, isotherms and heatlines for $\varphi = 0.1$ and $\phi = 60^\circ$ when $Ra = 10^3$ and 10^4. The rotation of the cavity with $\phi = 60^\circ$ on the counterclockwise causes the closed cell on the right top region of cavity becomes stronger and wider. For the enclosure with $Ra = 10^3$ (Fig. 4(a)) flow is not too strong in the enclosure since Rayleigh number is relatively small. Heat conduction is dominant mode of heat transfer in the cavity since no distortion is seen in isotherms. The domination of conduction heat transfer can also be observed from the heatline patterns since no passive area exists. The area of cavity can be divided into two parts from heat transfer point of view. The first part is the area in which heat is transferred from the hot to the cold wall. However, in the second part, heat is transferred from the middle to the top of the hot wall due to non-uniform wall temperature. This region is colored by dark gray. The increase of the Rayleigh number changes the heat and fluid flow patterns. As seen from Fig. 4(b), the increase of Rayleigh number from 10^3 to 10^4 enhances the strength of the flow and the area covered by the second closed cells becomes smaller. The steep distortions of isotherms in the cavity show relatively stronger convective heat transfer. The increase of Rayleigh number causes the clustering of heatlines from hot to the cold wall and generation of passive heat transfer area (white color) in which heat is rotated without having significant effect on heat transfer between walls.

Fig. 5 shows streamlines (left), isotherms (middle) and heatline (right) patterns for the cavity with $Ra = 10^5$ and $\varphi = 0.1$ when $\phi = 30^\circ$ and 60°. As seen from streamlines, the closed cells on the hot top wall exit for the cavity of $\phi = 30^\circ$ and 60°. The maximum streamfunction values (Ψ_{max}) for the enclosures of $\phi = 30^\circ$, 60° are 21.18 and 23.11. Steep distortions in the isotherms shows strong convective mode of heat transfer since $Ra = 10^5$. For the enclosures with $\phi = 30^\circ$ and 60°, a similar heatline patterns are observed. The values of Π_{min} and Π_{max} for the cavities of $\phi = 30^\circ$ are -3.85 and 2.85 while the same values for the cavity of $\phi = 60^\circ$ are -4.27 and 2.58 indicating increase of heat transfer through the enclosure.

Fig. 6 shows the variation of velocity profiles for different volume fractions at the mid-axis for $\phi = 0^\circ$ when $Ra = 10^3$, 10^4 and 10^5. The increase of Rayleigh number causes appearing of horizontal flows in the middle of the enclosure and increasing of V velocity components in the region near the wall. The increase of nanoparticle volume fraction does not change this trend, however the strength of fluid flow increases and the maximum and minimum V velocity components in the middle axes of enclosure with $\varphi = 0.1$ become greater than those of $\varphi = 0$ (clear fluids).

The variation of local Nusselt number along the hot wall for different volume fractions as $Ra = 10^3$, 10^4 and 10^5 are shown in Fig. 7 when $\phi = 0^\circ$. As seen from Fig. 7(a), the maximum local Nusselt number is at the bottom of hot wall having maximum temperature

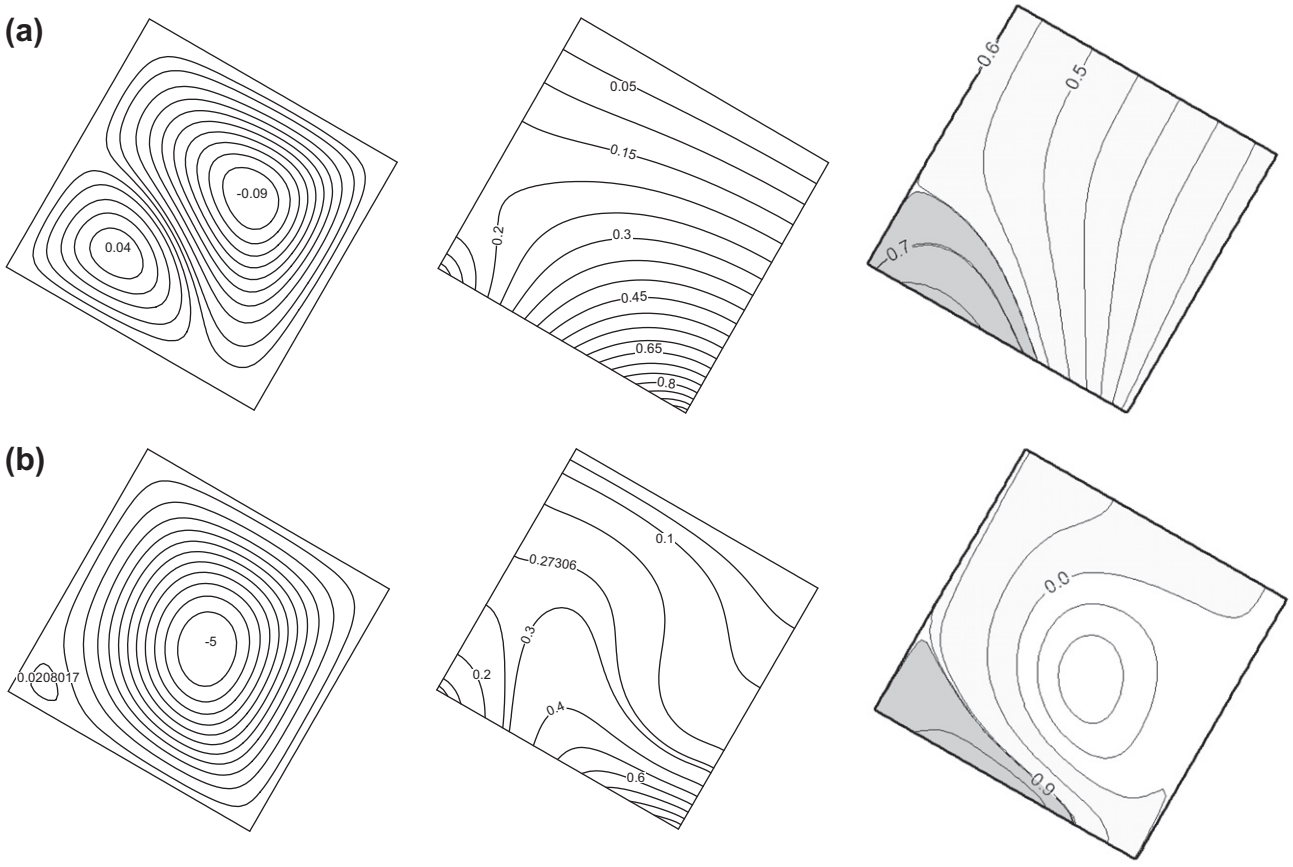

Fig. 4. Streamlines, isotherms and heatlines for $\varphi = 0.1$ and $\phi = 60^\circ$, (a) $Ra = 10^3$ and (b) $Ra = 10^4$.

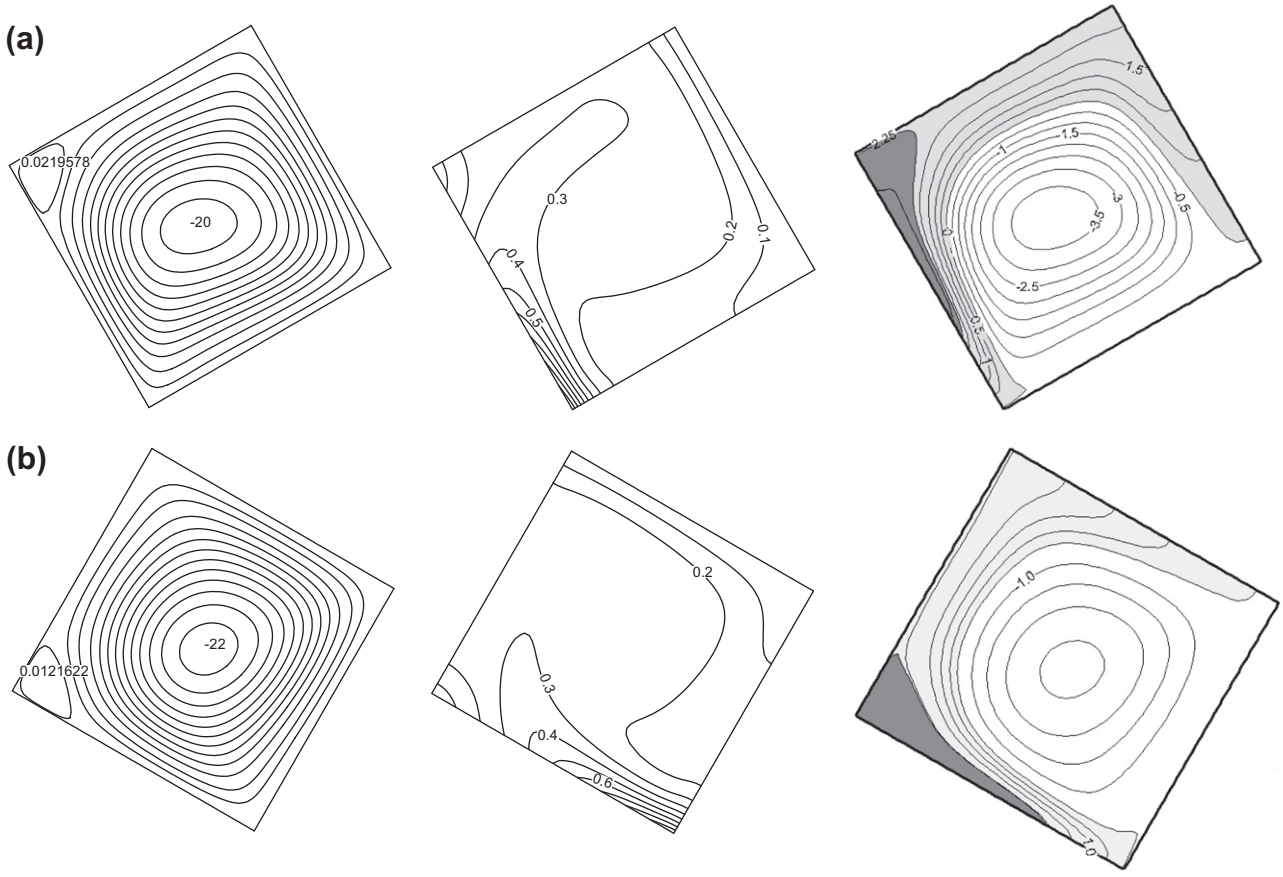

Fig. 5. Streamlines (on the left), isotherms (on the right) and heatlines (on the right) for Ra = 10^5 when $\varphi = 0.1$, (a) $\phi = 30°$ and (b) $\phi = 60°$.

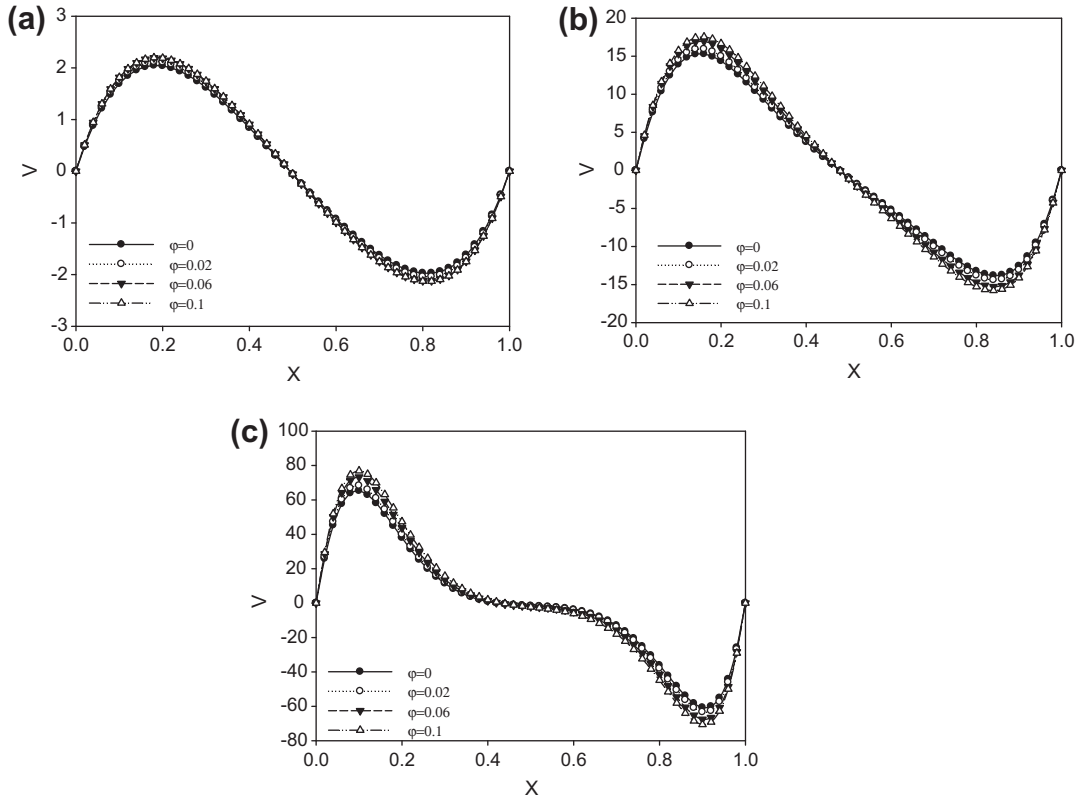

Fig. 6. Variation of velocity profiles for different volume fractions at the mid-axis for $\phi = 0°$, (a) Ra = 10^3, (b) Ra = 10^4 and (c) Ra = 10^5.

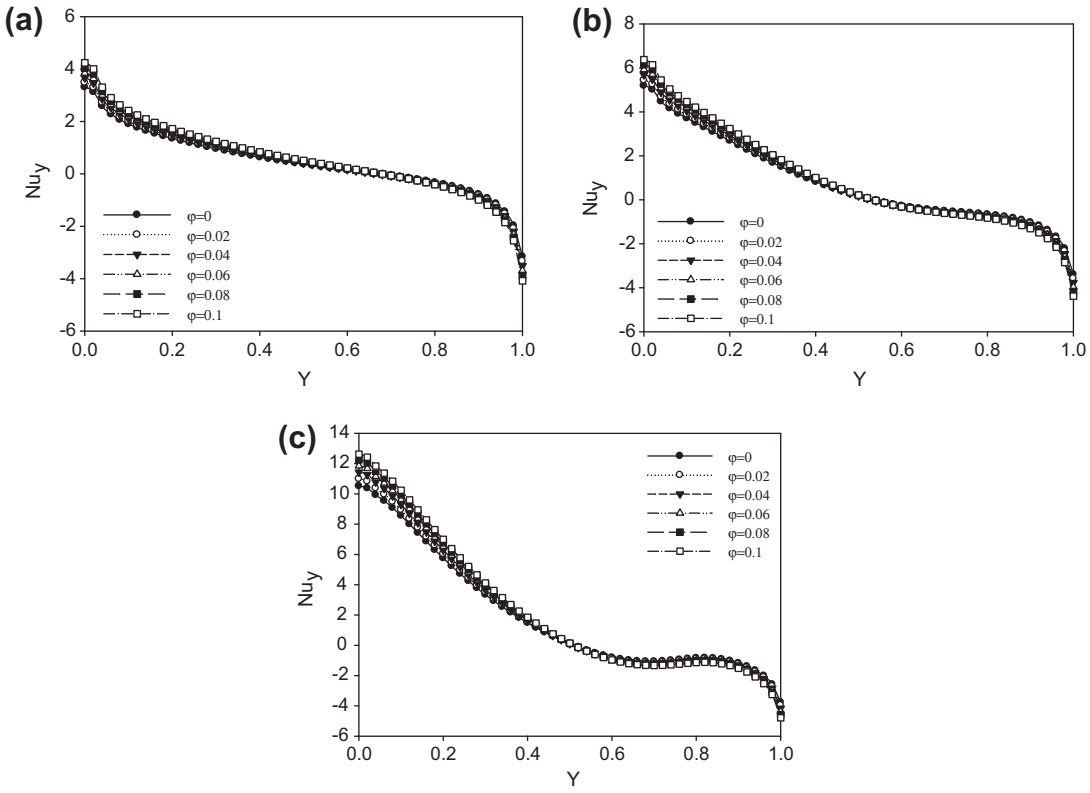

Fig. 7. Variation of local Nusselt number along the hot wall for different volume fractions at $\phi = 0°$, (a) Ra = 10^3, (b) Ra = 10^4 and (c) Ra = 10^5.

of the enclosure. By decreasing of temperature along the hot wall, the local Nusselt number also decreases and after a point, the local Nusselt number receives negative values refers to the reverse heat transfer (i.e., heat transfer from fluid to the wall). The minimum Nusselt number is observed at the top of the hot wall showing maximum heat transfer from the fluid to the hot wall. The increase of the nanoparticle volume fraction does not change this trend; however local Nusselt number slightly increases with increase of nanoparticle volume fraction, particularly at the top region of hot wall. The same trend is observed in Fig. 7(b) and (c) showing the local Nusselt number for Ra = 10^4 and 10^5. As expected, the absolute value of local Nusselt number increases with increase of the Rayleigh number as well as the increase of nanoparticle volume fraction.

Variation of local Nusselt number (i.e., Nu_y) along the hot wall of enclosures with different angles and Rayleigh numbers (Ra = 10^3, 10^4 and 10^5) when $\varphi = 0.1$ are shown in Fig. 8. For the enclosure with Ra = 10^3, the local Nusselt number of the hot wall does not vary with inclination angle as seen from Fig. 8(a) due to the dominant conduction mode of heat transfer. By increase of Rayleigh number, the convective heat transfer becomes stronger and the variation of local Nusselt number for $\phi = 90°$ becomes different than the variation of the hot wall local Nusselt number of enclosures with $\phi = 0°$, 30° and 60°. The increase of Rayleigh number to 10^5 improves the effect of convection heat transfer in the enclosure. Hence, the variations of local Nusselt number of hot walls become different from each others. The interesting point of Fig. 8(c) is that the local Nusselt number of the enclosure with $\phi = 60°$ is lower than those of enclosures of $\phi = 0°$ and 30°. Hence, a decrease in the average Nusselt number of the enclosure with of $\phi = 60°$ may be expected. Fig. 8(c) also shows that the local Nusselt number of the most part of the hot wall is positive when $\phi = 90°$ showing the heat transfer from the hot to the cold wall. A small part of the hot wall receives heat transfer from the fluid. Hence, an improvement in the average Nusselt number of the enclosure with $\phi = 90°$ may be expected.

Fig. 9 is presented to observe the effect of nanoparticle volume fraction on heat transfer through the enclosure. The variation of local Nusselt number of the cold wall $Nu_c$and the normalized local Nusselt numbers for different nanoparticle volume fraction are shown in the same figure. As expected, the maximum local Nusselt is observed at the region of $y = 1$ of the cold wall and the local Nusselt number decreases toward the bottom of the cold wall. The increase of the nanoparticle volume fraction increases local Nusselt number. The value of the normalized Nusselt number is around 1.05 and 1.1 for the enclosures with $\varphi = 0.02$ and 0.04. The increase of nanoparticle volume fraction enhances heat transfer at the bottom of the cold wall more than top region. This might be due to enhance of conduction mode of heat transfer in the bottom region of the enclosure. Fig. 9 clearly shows that the increase of nanoparticle volume fraction increases heat transfer in the enclosure and the maximum enhancement of heat transfer is observed for $\varphi = 0.1$.

The effect of Rayleigh number and nanoparticle volume fraction on average Nusselt number of the enclosures with $\phi = 0°$ are shown in Table 1. The average Nusselt number increases with increase of Rayleigh number since the convective heat transfer is enhanced. Moreover, the increase of the nanoparticle volume fraction improves heat transfer in the enclosure and consequently average Nusselt number increases. The rate of increase of average Nusselt number with nanoparticle volume fraction may be understood better from Table 2 in which the normalized average Nusselt numbers of different enclosures are presented. The rate of increase for the enclosures with Ra = 10^4 and 10^5 are almost the same and normalized average Nusselt number attains 1.19 for $\varphi = 0.1$. This means that the adding of the nanoparticle improves heat transfer around 20% for the cavities with Ra = 10^4 and 10^5. The normalized average Nusselt number for Ra = 10^3 are greater Ra = 10^4 and 10^5. The increase of heat transfer

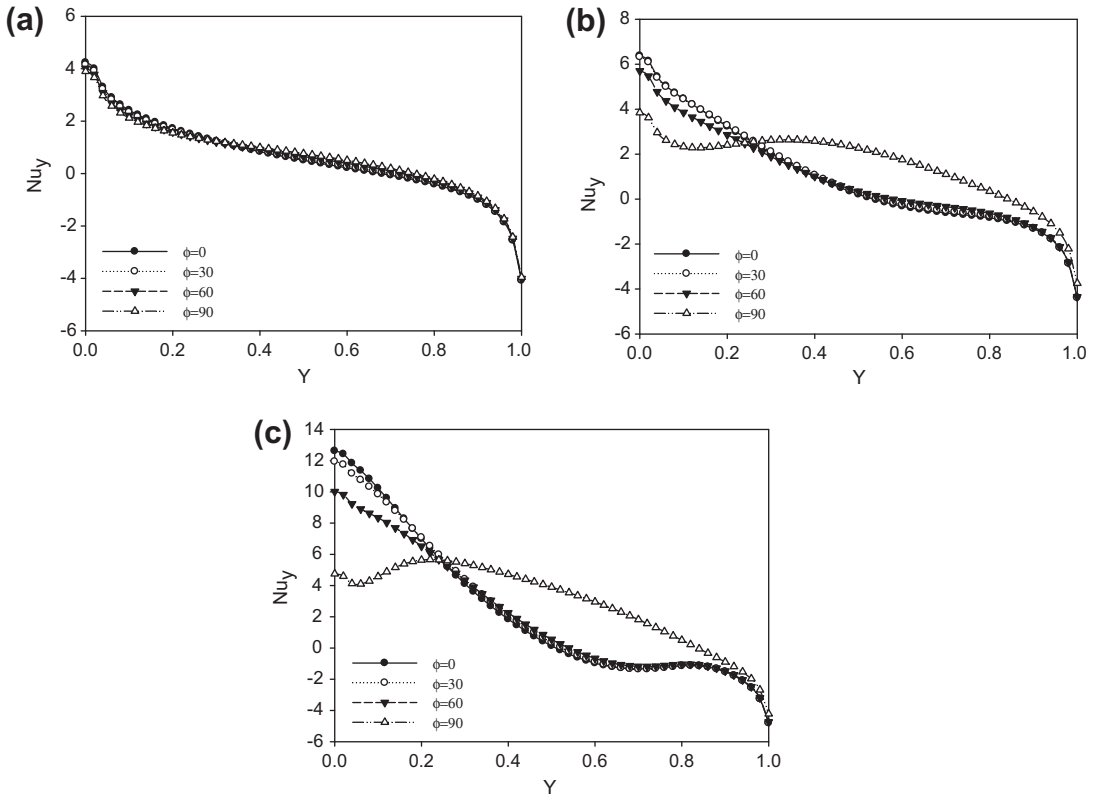

Fig. 8. Variation of local Nusselt number along the hot wall for $\varphi = 0.1$ at different inclination angles, (a) Ra = 10^3, (b) Ra = 10^4 and (c) Ra = 10^5.

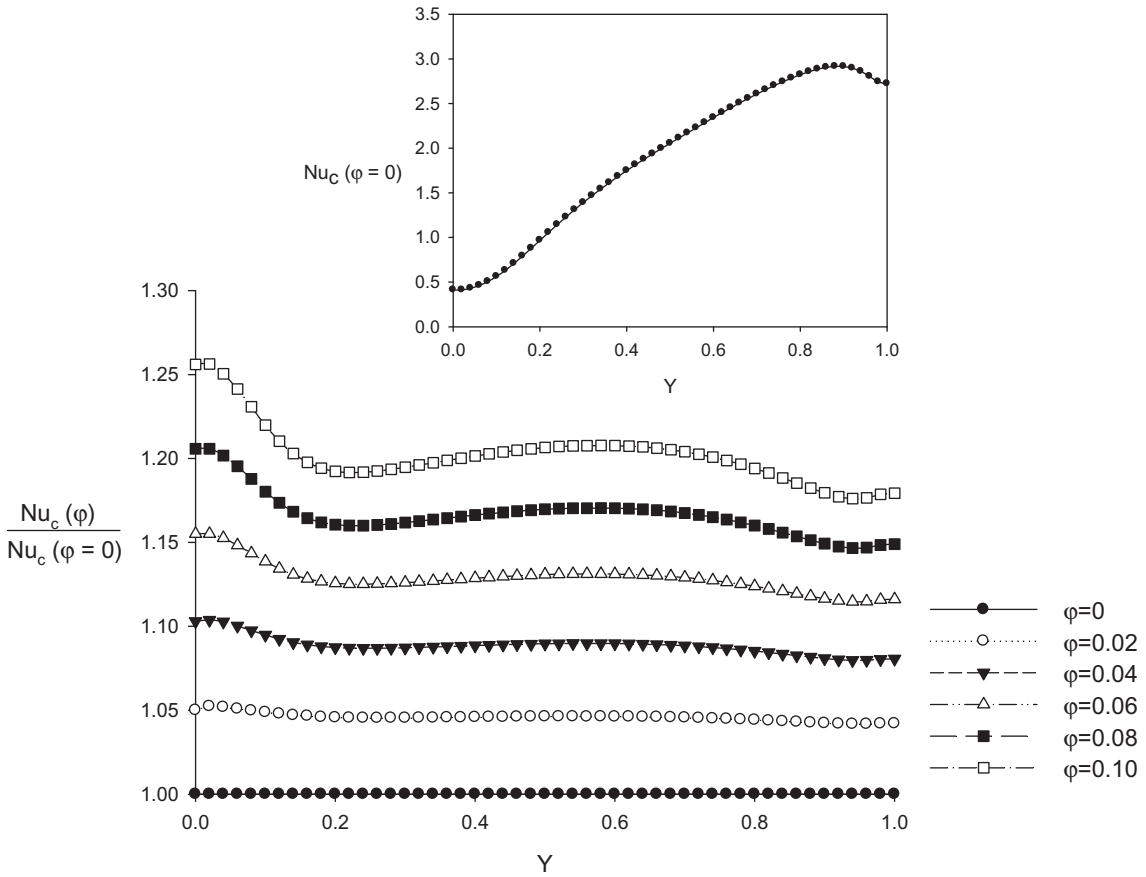

Fig. 9. Variation of normalized local Nusselt number along the cold wall for different values of nano particle volume fraction when $\phi = 0^\circ$ and Ra = 10^5.

Table 1
Average Nusselt number Nu_{avg} for a cavity with $\phi = 0°$.

Ra	$\varphi = 0$	$\varphi = 0.02$	$\varphi = 0.04$	$\varphi = 0.06$	$\varphi = 0.08$	$\varphi = 0.10$
10^3	0.47	0.49	0.52	0.55	0.58	0.61
10^4	0.79	0.83	0.86	0.89	0.92	0.95
10^4	1.92	2.00	2.08	2.16	2.23	2.29

Table 2
Normalized average Nusselt number Nu_{avg} for a cavity with $\phi = 0°$.

Ra	$\varphi = 0$	$\varphi = 0.02$	$\varphi = 0.04$	$\varphi = 0.06$	$\varphi = 0.08$	$\varphi = 0.10$
10^3	1.00	1.06	1.11	1.17	1.24	1.30
10^4	1.00	1.05	1.09	1.13	1.16	1.19
10^5	1.00	1.04	1.08	1.12	1.16	1.19

Table 3
Average Nusselt number Nu_{avg} for different inclination angles ϕ at different nanoparticle volume fraction φ.

Ra	$\phi = 30°$			$\phi = 60°$			$\phi = 90°$		
	$\varphi = 0$	$\varphi = 0.06$	$\varphi = 0.10$	$\varphi = 0$	$\varphi = 0.06$	$\varphi = 0.10$	$\varphi = 0$	$\varphi = 0.06$	$\varphi = 0.10$
10^3	0.474	0.557	0.618	0.493	0.578	0.64	0.536	0.622	0.682
10^4	0.836	0.937	0.989	0.765	0.852	0.891	1.286	1.454	1.546
10^5	1.925	2.168	2.309	1.727	1.952	2.086	2.398	2.733	2.943

for an enclosure with Ra = 10^3 by adding CuO nanoparticle attains to 30%. Table 2 reveals that the effect of nanoparticle on enhancement heat transfer in the enclosures with the low Rayleigh number is greater than with high Rayleigh number.

The effects of inclination angle on average Nusselt number of enclosures with different nanoparticle volume fraction and Rayleigh numbers are shown in Table 3. The average Nusselt number increases with increase of nanoparticle volume fraction for enclosures with $\phi = 30°$, 60° and 90°. For enclosures with Ra = 10^3, the increase of inclination angle increases average Nusselt number. However, for the enclosures with Ra = 10^4 and 10^5, the increase of inclination angle from and $\phi = 30°$ to 60° reduces average Nusselt number. For the same enclosures, the increase of inclination angles from $\phi = 60°$ to 90° improves heat transfer. Hence, for the considered enclosure with Ra = 10^4 and 10^5 and the ranges of ϕ and φ studied in the present paper, the minimum heat transfer in the cavity is observed for the enclosures with $\phi = 60°$ and $\varphi = 0$ (classical fluids).

8. Conclusions

Heatline visualization technique is used to visualize the heat transport in a non-isothermally heated square inclined enclosure filled with water based CuO nanofluid. Some concluding remarks can be drawn from the present study as follows:

(a) The heat transfer in the cavity increases by adding nanoparticles, however the rate of increase is greater for the enclosures with low Rayleigh number in which conduction heat transfer is more dominant.
(b) Visualization of heatline is successfully adapted to nanoparticle convective flows. The path of heat transfer in the enclosure is successfully observed for different nanoparticle volume fraction.
(c) Small closed cells occur in the top of hot wall of enclosures with zero inclination angles due to non uniform hot wall temperature.
(d) For the enclosures with Ra = 10^3, two kinds of heatline patterns exist in the enclosure. The first one shows heat transfer from the bottom region of hot wall to the cold wall and the second one resembles heat transfer from the middle region to the top region of the hot wall. For the enclosure with Ra = 10^4 and 10^5, three different heat transfer regions are observed. In addition to heat transfer between the hot and cold walls and the hot wall with itself, a passive heat transfer region is observed in which heat rotates and this area does not have any effect on heat transfer between the hot and cold walls.
(e) For the enclosure with Ra = 10^3 , the increase of inclination angle increases Nusselt number while for the enclosures with Ra = 10^4 and 10^5, the average Nusselt number decrease with the increase of inclination angle from 30° to 60° and then it increases with the increase of inclination angle from 60° to 90°.
(f) For the considered enclosure and studied ranges of Rayleigh, nanoparticle volume fraction and inclination angles, maximum Nusselt number is observed for the cavity with Ra = 10^5, $\phi = 90°$ and $\varphi = 0.1$ as 2.943 while the minimum average Nusselt number belongs to the enclosure with Ra = 10^3, $\phi = 0°$ and $\varphi = 0$ as 0.474.

References

[1] S. Kakac, A. Pramuanjaroenkij, Review of convective heat transfer enhancement with nanofluids, Int. J. Heat Mass Transfer 52 (2009) 3187–3196.
[2] W. Daungthongsuk, S. Wongwises, A critical review of convective heat transfer nanofluids, Renew. Sustain Energy Rev 11 (2007) 797–817.
[3] V. Trisaksri, S. Wongwises, Critical review of heat transfer characteristics of nanofluids, Renew. Sustain. Energy Rev. 11 (2007) 512–523.
[4] X.Q. Wang, A.S. Mujumdar, Heat transfer characteristics of nanofluids: a review, Int. J. Therm. Sci. 46 (2007) 1–19.
[5] N. Putra, W. Roetzel, S.K. Das, Natural convection of nanofluids, Heat Mass Transfer 39 (2003) 775–784.
[6] R. Saidur, K.Y. Leong, H.A. Mohammad, A review on applications and challenges of nanofluids, Renew. Sustain. Energy Rev. 15 (2011) 1646–1668.
[7] S. Lee, U.S. Choi, S. Li, J.A. Eastman, Measuring thermal conductivity of fluids containing oxide nanoparticles, ASME J. Heat Transfer 121 (1999) 280–289.
[8] J.A. Eastman, U.S. Choi, S. Li, W. Yu, L.J. Thompson, Anomalously increased effective thermal conductivity of ethylene glycol-based nanofluids containing copper nanoparticles, Appl. Phys. Lett. 78 (2001) 718–720.
[9] H.F. Oztop, E. Abu-Nada, Numerical study of natural convection in partially heated rectangular enclosure filled with nanofluids, Int. J. Heat Fluid Flow 29 (2008) 1326–1336.
[10] E. Bilgen, Y.R. Ben, Natural convection in enclosure with heating and cooling by sinusoidal temperature profiles on one side, Int. J. Heat Mass Transfer 50 (2007) 139–150.
[11] E. Natarajan, T. Basak, S. Roy, Natural convection flows in a trapezoidal enclosure with uniform and non-uniform heating of bottom wall, Int. J. Heat Mass Transfer 51 (2008) 747–756.
[12] A. Dalal, M.K. Das, Natural convection in a cavity with a wavy wall heated from below and uniformly cooled from the top and both sides, ASME J. Heat Transfer 128 (2006) 717–725.
[13] T. Basak, S. Roy, A.R. Balakrishnan, Effect of thermal boundary conditions on natural convection flow in a square cavity, Int. J. Heat Mass Transfer 49 (2006) 4525–4535.
[14] Y. Varol, H.F. Öztop, I. Pop, Numerical analysis of natural convection for a porous rectangular enclosure with sinusoidally varying temperature profile on the bottom wall, Int. Commun. Heat Mass Transfer 35 (2008) 56–64.
[15] I.E. Sarris, I. Lekakis, N.S. Vlachos, Natural convection in a 2D enclosure with sinusoidal upper wall temperature, Numer. Heat Transfer, Part A: Appl. 42 (2002) 513–530.
[16] H.F. Oztop, E. Abu-Nada, Y. Varol, K. Al-Salem, Computational analysis of non-isothermal temperature distribution on natural convection in nanofluid filled enclosures, Superlattices Microstruct. 49 (2011) 453–467.

[17] S. Kimura, A. Bejan, The heatline visualization of convective heat transfer, ASME J. Heat Transfer 105 (1983) 916–919.
[18] V.A.F. Costa, Bejan's heatlines and masslines for convection visualization and analysis, Appl. Mech. Rev. 59 (2006) 126–145.
[19] E. Hakyemez, M. Mobedi, H. Oztop, Effects of wall-located heat barrier on conjugate conduction/natural-convection heat transfer and fluid flow in enclosures, Numer. Heat Transfer Part A: Appl. 54 (2008) 197–220.
[20] Y. Varol, H.F. Oztop, M. Mobedi, I. Pop, Visualization of natural convection heat transport using heatline method in porous non-isothermally heated triangular cavity, Int. J. Heat Mass Transfer 51 (2008) 5040–5051.
[21] T. Basak, S. Roy, A. Matta, I. Pop, Analysis of heatlines for natural convection within porous trapezoidal enclosures: effect of uniform and non-uniform heating of bottom wall, Int. J. Heat Mass Transfer 53 (2010) 5947–5961.
[22] E. Abu-Nada, Application of nanofluids for heat transfer enhancement of separated flows encountered in a backward facing step, Int. J. Heat Fluid Flow 29 (2008) 242–249.
[23] K. Khanafer, K. Vafai, M. Lightstone, Buoyancy-driven heat transfer enhancement in a two dimensional enclosure utilizing nanofluids, Int. J. Heat Mass Transfer 46 (2003) 3639–3653.
[24] A. Akbarinia, A. Behzadmehr, A numerical study of laminar mixed convection of a nanofluid in horizontal curved tubes, Appl. Therm. Eng. 27 (2007) 1327–1337.
[25] S.E.B. Maiga, S.J. Palm, C.T. Nguyen, G. Roy, N. Galanis, Heat transfer enhancement by using nanofluids in forced convection flows, Int. J. Heat Fluid Flow 26 (2005) 530–546.
[26] H.C. Brinkman, The viscosity of concentrated suspensions and solutions, J. Chem. Phys. 20 (1952) 571–581.
[27] S.V. Patankar, Numerical Heat Transfer and Fluid Flow, Hemisphere Publishing Corporation Taylor and Francis Group, New York, 1980.
[28] H.K. Versteeg, W. Malalasekera, An Introduction to Computational Fluid Dynamic: The Finite Volume Method, John Wiley & Sons Inc., New York, 1995.
[29] A. Al-Sarkhi, E. Abu-Nada, Characteristics of forced convection heat transfer in vertical internally finned tube, Int. Commun. Heat Mass Transfer 32 (2005) 557–564.
[30] E. Abu-Nada, Effects of variable viscosity and thermal conductivity of CuO-Water nanofluid on heat transfer enhancement in natural convection: mathematical model and simulation, J. Heat Transfer 132 (2010) 052401.